NUMERICAL MODELLING OF MECHANICAL RESPONSE OF A TWO-PHASE COMPOSITE

Eligiusz Postek[1], Tomasz Sadowski[2] and Stephen Hardy[1]
[1]School of Engineering, University of Wales Swansea, Singleton Park SA2 8PP Swansea, Wales UK; [2]Faculty of Civil and Sanitary Engineering, Lublin University of Technology, ul. Nadbystrzycka 40, 20-618 Lublin, Poland

Abstract: The presentation considers behaviour of two-phase composite material. According to experimental observations (SME imaging) this type of composites can be considered as polycrystals consisting of grains and thin intergranular layers. A representative volume element (RVE) has been analysed taking into account its internal structure. The analysis is carried out using FE technique. The technique is applied to obtain mascroscopic stresses distribution due to initial defects embedded in the intergranular layers of the sample (RVE).

Key words: ceramics; interfaces; finite strains;

1. INTRODUCTION

A typical application of polycrystalline materials is the fabrication of cutting tools. The tools are working in such severe conditions as high dynamic and temperature loadings. An exemplary two-phase material used for them may consist of elastic grains and ductile interfaces. The interfaces are thick enough not to be treated as only contacting adhesive layers. Our interest will focus on the behavior of the relatively thick intergranular layers which affect performance of entire sample.

An example of SME image showing grains, interfaces and their ideogramic idealization are presented in Figure 1. The grains can exhibit anisotropic behavior.
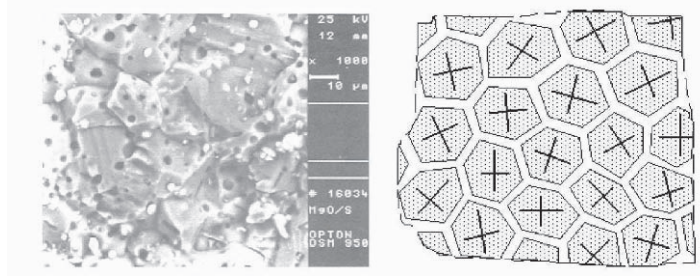
Figure 1. SME image of a polycrystal (left), idealization (right).

2. MATHEMATICAL FORMULATION

The problem is elasto-plastic with the assumption of large displacements (Owen and Hinton, 1980; Bathe, 1996). We consider nonlinear terms of the strain tensor. The virtual work equation is of the form

$$\delta\Pi = \int_{\Omega^o} {}^{t+\Delta t}_{o}\mathbf{S} \cdot \delta\,{}^{t+\Delta t}_{o}\mathbf{E}\,d\Omega^o - \int_{\Omega^o} {}^{t+\Delta t}\mathbf{f}\delta\,{}^{t+\Delta t}\mathbf{u}\,d\Omega^o - \int_{\partial\Omega^o_\sigma} {}^{t+\Delta t}\mathbf{t}\delta\,{}^{t+\Delta t}\mathbf{u}\,d\left(\partial\Omega^o_\sigma\right) \quad (1)$$

where **S** and **E** are the II Piola-Kirchhof stress tensor and Green Lagrange strains, **f**, **t** and **u**={u,v,w} are body forces, boundary tractions and displacements. All of the quantities are determined at time t+Δt in the initial configuration. To obtain the above equation at time $t+\Delta t$ in the configuration at time t the relations (Malvern, 1969; Crisfield, 1991) are used

$$ {}^{t+\Delta t}_{o}\mathbf{S} = \frac{\rho}{\rho_o}\,{}^{t+\Delta t}_{t}\mathbf{S}, \quad {}^{t+\Delta t}_{o}\mathbf{E} = \frac{\rho}{\rho_o}\,{}^{t+\Delta t}_{t}\mathbf{E}, \quad \rho\,d\Omega^t = \rho_o\,d\Omega^o \quad (2)$$

$$\int_{\Omega^t} {}^{t+\Delta t}_{t}\mathbf{S} \cdot \delta\,{}^{t+\Delta t}_{t}\mathbf{E}\,d\Omega^t = \int_{\Omega^t} {}^{t+\Delta t}\mathbf{t}\delta\,{}^{t+\Delta t}\mathbf{u}\,d\Omega^t + \int_{\partial\Omega^t_\sigma} {}^{t+\Delta t}\mathbf{t}\delta\,{}^{t+\Delta t}\mathbf{u}\,d\left(\partial\Omega^t_\sigma\right) \quad (3)$$

Now, we apply incremental decomposition to the quantities in the equation above: strains, ${}^{t+\Delta t}_{t}\mathbf{E}={}^{t}_{t}\mathbf{E} + \Delta\mathbf{E}$, stresses ${}^{t+\Delta t}_{t}\mathbf{S}={}^{t}_{t}\mathbf{S} + \Delta\mathbf{S}$, displacements, ${}^{t+\Delta t}\mathbf{u}={}^{t}\mathbf{u} + \Delta\mathbf{u}$, forces ${}^{t+\Delta t}\mathbf{f}={}^{t}\mathbf{f} + \Delta\mathbf{S}$, ${}^{t+\Delta t}\mathbf{t}={}^{t}\mathbf{t} + \Delta\mathbf{t}$. Since the II P-K tensor at time t in the configuration t is equal to the Cauchy stress tensor ${}^{t}_{t}\mathbf{S}={}^{t}_{t}\boldsymbol{\tau}$ the stress decomposition is of the form ${}^{t+\Delta t}_{t}\mathbf{S}={}^{t}_{t}\boldsymbol{\tau} + \Delta\mathbf{S}$.

Then, we employ the following strain increment decomposition into its linear and nonlinear parts $\Delta\mathbf{E} = \Delta\mathbf{e} + \Delta\boldsymbol{\eta}$, , $\Delta\mathbf{e} = \overline{\mathbf{A}}\Delta\mathbf{u}$, $\Delta\boldsymbol{\eta} = \mathbf{A}(\Delta\mathbf{u}')\Delta\mathbf{u}'/2$,

where $\Delta\mathbf{u}$' is the vector of the displacement increment derivatives w.r.t. Cartesian coordinates and ($\mathbf{A}$, $\overline{\mathbf{A}}$) are the linear and nonlinear operators, Bathe (1996). Substituting the described relations, into the virtual work equation, Eqn 3, and assuming that the equation is precisely fulfilled at the end of the step we obtain the following incremental form of the virtual work equation

$$\int_{\Omega^t}\left(_t^t\boldsymbol{\tau}\cdot\delta\boldsymbol{\eta} + \Delta\mathbf{S}\cdot\delta\Delta\mathbf{e}\right)d\Omega^t = \int_{\Omega^t}\Delta\mathbf{f}\,\delta\Delta\mathbf{u}\,d\Omega^t + \int_{\partial\Omega^t_\sigma}\Delta\mathbf{t}\,\delta\Delta\mathbf{u}\,d\left(\partial\Omega^t_\sigma\right)\ (4)$$

Employing the finite element approximation $\Delta\mathbf{u} = \mathbf{N}\Delta\mathbf{q}$ and $\Delta\mathbf{u}' = \mathbf{B}'_L\Delta\mathbf{q}$, where $\mathbf{N}$ is the set of shape functions and $\Delta\mathbf{q}$ is the increment of nodal displacements and considering the following set of equalities

$$_t^t\boldsymbol{\tau}^T\delta\boldsymbol{\eta} = {}_t^t\boldsymbol{\tau}\delta\left(\overline{\overline{\mathbf{A}}}\right)\Delta\mathbf{u}' = \delta(\Delta\mathbf{u}')^T{}_t^t\overline{\boldsymbol{\tau}}\,\Delta\mathbf{u}' = \delta(\Delta\mathbf{q})^T{}_t^t\overline{\boldsymbol{\tau}}\mathbf{B}'_L \qquad (5)$$

where $_t^t\overline{\boldsymbol{\tau}}$ is the Cauchy stress matrix

$$_t^t\overline{\boldsymbol{\tau}} = \begin{bmatrix} _t^t\underline{\boldsymbol{\tau}} & & \\ & _t^t\underline{\boldsymbol{\tau}} & \\ & & _t^t\underline{\boldsymbol{\tau}} \end{bmatrix} \qquad _t^t\underline{\boldsymbol{\tau}} = \begin{bmatrix} _t^t\sigma_{xx} & _t^t\tau_{xy} & _t^t\tau_{xz} \\ & _t^t\sigma_{yy} & \tau_{yz} \\ & & _t^t\sigma_{zz} \end{bmatrix} \qquad (6)$$

we obtain the following discretized form of the virtual work equation

$$\left(\int_{\Omega^t}\mathbf{B}'_L{}^T{}_t^t\overline{\boldsymbol{\tau}}\mathbf{B}'_L\,d\Omega^t\right)\Delta\mathbf{q} + \int_{\Omega^t}\mathbf{B}_L^T\Delta\mathbf{S}\,d\Omega^t = \int_{\Omega^t}\mathbf{N}^T\Delta\mathbf{f}\,d\Omega^t + \int_{\partial\Omega^t_\sigma}\mathbf{N}^T\Delta\mathbf{t}\,d\left(\partial\Omega^t_\sigma\right) (7)$$

Now, we will deal with the constitutive model and employ the linearized constitutive equation, in fact with the stress increment $\Delta\mathbf{S}$.

2.1   Finite strains

When considering the finite strains effect (Pinsky et al., 1983), the gradient $\mathbf{F} = \partial(\mathbf{X} + \mathbf{u})/\partial\mathbf{X}$ is decomposed into its elastic and plastic parts, $\mathbf{F} = \mathbf{F}^e\mathbf{F}^p$, Figure 1. To integrate the constitutive relations the deformation increment $\Delta\mathbf{D}$ is rotated to the unrotated configuration by means of rotation matrix obtained from polar decomposition $\mathbf{F} = \mathbf{VR} = \mathbf{RU}$,

$\Delta \mathbf{d} = \mathbf{R}_{n+1}^{T} \Delta \mathbf{D} \mathbf{R}_{n+1}$, then the radial return is performed and stresses are transformed to the Cauchy stresses at $n+1$, $\boldsymbol{\sigma}_{n+1} = \mathbf{R}_{n+1} \boldsymbol{\sigma}_{n+1}^{u} \mathbf{R}_{n+1}^{T}$. The stresses are integrated using the consistent tangent matrix Simo and Taylor (1985) and the integration is done in the unrotated configuration as for small strains.
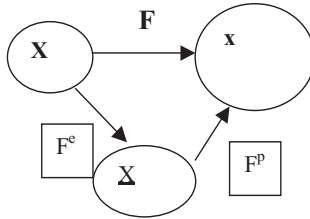

Figure 2. Elastic and plastic gradient decomposition.

3.   NUMERICAL RESULTS

The mechanical properties of the polycrystal consisting of elastic grains and metallic interfaces are as follows: grains; Young's modulus 4.1×10^{11} Pa and Poisson's ratio 0.25, interfaces: Young modulus 2.1×10^{11} Pa, Poisson's ratio 0.235, yield limit 2.97×10^{11} Pa and small hardening modulus 1.0×10^{6} Pa. The dimensions of the sample are 100x100x10 μm. The scheme of the Representative Volume Element (RVE) is given in Figure 3.
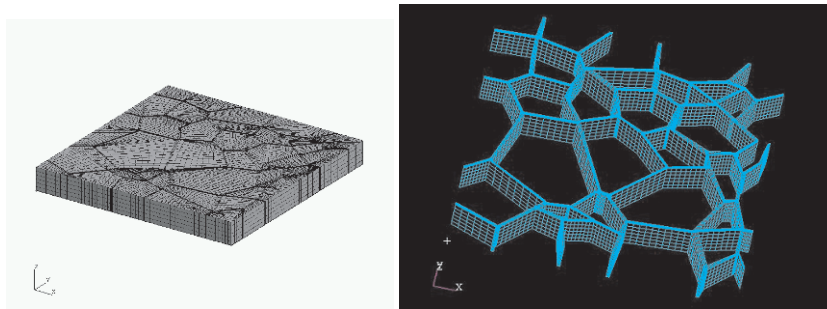

Figure 3. Mesh of representative volume element (left), interfaces (right).

The sample is discretized with 48894 elements and 58016 nodes. The sample is fixed on one side and loaded with the uniform pressure of 400 MPa on the other one. There is imposed symmetry condition in the bottom

of the sample. Since the grains are elastic the sample fails due to large plastic strains occurring in the elasto-plastic interfaces. The displacement fields just before "first yield" and before failure are shown in Figure 4, left and right, respectively.
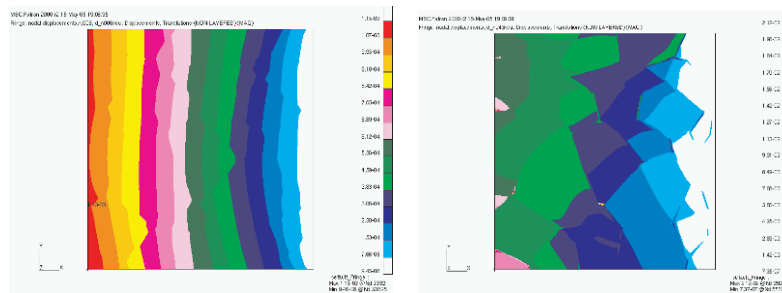

Figure 4. Displacement fields, before "first yield" (left) and before failure (right).

There is demonstrated qualitative difference between the two situations. The displacement field just before yielding exhibits discontinuities along interfaces (Figure 4, left). It can be interpreted that the grains tend to slide along the interfaces. Figure 4 (right) shows that the grains are strongly displaced and rotated. We may notice that the failure is spatial (Figure 5), namely the ductile material of the interfaces is squeezed be the stiff grains and pushed out from the sample. The crucial place appeared to be a very short segment of the interface parallel to the loading axis. The segment connects four other interfaces and is located between four grains.
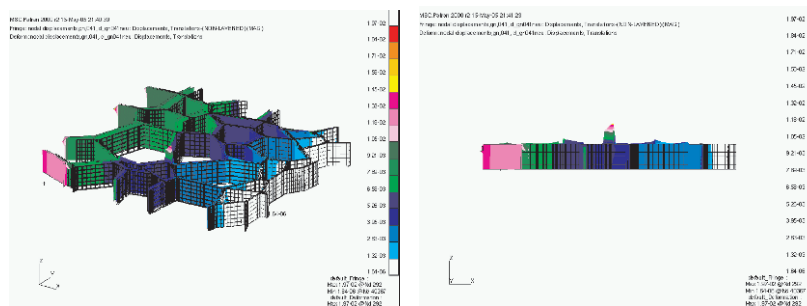

Figure 5. Failure of the interfaces, spatial view (left), side view (right).

Mises stresses distribution just before "first yield" and before failure are presented in Figure 6. Looking at the map of the von Mises stresses

distribution before "first yield" we may see clearly the discontinuities in the interfaces, the stresses are lower in the interfaces than in the grains (Figure 6, left). Qualitatively similar picture of the von Mises stresses is shown in Figure 6, right. This is the situation just before failure. The von Mises stresses are much higher in the grains and relatively low (a little above yield limit due to hardening) in the interfaces, therefore, the discontinuities become stronger.
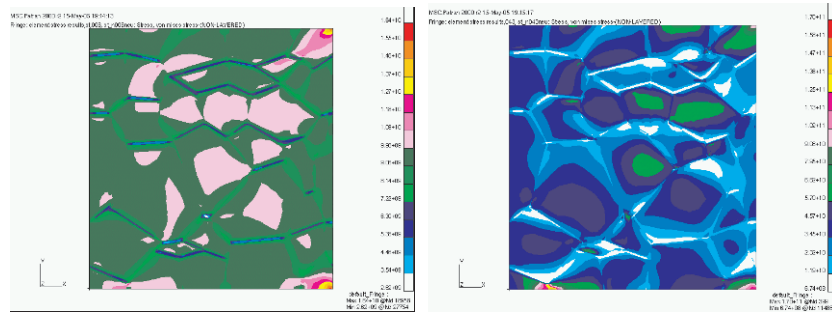

Figure 6. Von Mises stresses distributions, before "first yield" (left), before failure (right).

Now, we will present the distributions of equivalent plastic strains showing their maps in the entire polycrystal and in the interfaces. The equivalent plastic strains distributions just after "first yield" are shown in Figure 7 and before failure in Figure 8.
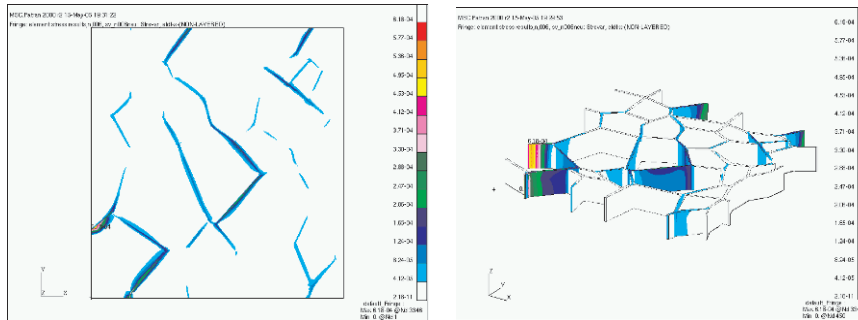

Figure 7. Equivalent plastic strains after "first yield", polycrystal (left), interfaces (right).

When comparing Figures 7 and 8 we may notice that the distribution of equivalent plastic strains is qualitatively different after first yield and before failure. In the case of "first yield" (Figure 7) the interfaces are getting plastic relatively uniformly and the already plastic interfaces are arranged approximately in the angle of 45°. The situation becomes different before

failure when the plastic strains are redistributed and strongly localized (Figure 8) close to connections of the interfaces and in this particular case the highest plastic strains are in the interface segment corresponding to the one which is seen in Figure 5 and decides about the failure.
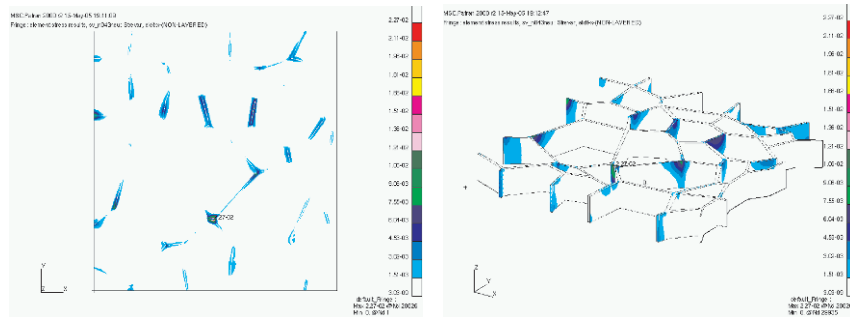

Figure 8. Equivalent plastic strains before failure, polycrystal (left), interfaces (right).
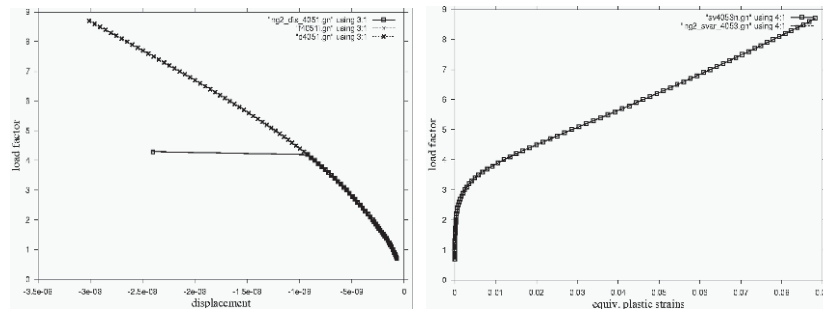

Figure 9. Displacement versus load factor (left), equivalent plastic strains versus load factor. (right).

The load versus displacement curves are presented in Figure 9 (left). A horizontal displacement along the loading axis in the middle of the loaded face of the sample is chosen There are considered three cases, namely, elasto-plastic (thick crosses), elasto-plastic and included geometrical imperfection (thin crosses), elasto-plastic and nonlinear geometry. A small geometric imperfection is included in the one of the interfaces in the middle of the sample. We may see that when concerning this particular model the influence of the imperfection is not significant. The influence of the nonlinear geometry is important since it decides about the load carrying

capacity of the sample. The load factor of the load carrying capacity load is 4.0. The two curves in Figure 9 (right) show the dependence of the equivalent plastic strains on loading factor. Two cases are considered, namely, the elasto-plastic analysis and elasto-plastic analysis including nonlinear geometry. The curves for both cases are practically covering each other until the failure point at load multiplier 4.0.

4.   FINAL REMARKS

The communication focuses on the problem of load carrying capacity and failure mode of an RVE of a polycrystallic material. The most characteristic features of the failure mode are the grains rotations and spatial displacing of the interface material. The results show also the necessity of including the nonlinear geometry into the analysis.

ACKNOWLEDGMENTS

REFERENCES

Owen D. R. J., Hinton E., 1980, Finite Elements in Plasticity, Pineridge Press.

Bathe K. J., 1996, Finite Element Procedures, Prentice Hall.

Malvern, L. E., 1969, Introduction to the Mechanics of Continuous Medium, Prentice Hall.

Crisfield, M. A., 1991, Non-linear Finite Element Analysis of Solids and Structures, John Wiley.

Pinsky, P.M., Ortiz, M., Pister, K.S., Numerical integration of rate constitutive equations in finite deformations analysis, *Computer Methods in Applied Mechanics and Engineering,* 40 (2), 1983:137-158.

Simo, J.C., Taylor, R.L., Consistent tangent operators for rate independent elastoplasticity, *Computer Methods in Applied Mechanics and Engineering*, 48(1), 1985: 101-118.